RSC Advances

PAPER

View Article Online
View Journal | View Issue

Cite this: *RSC Adv.*, 2024, **14**, 24165

Binding uric acid: a pure chemical solution for the treatment of hyperuricemia†

Yun-Yun Li,‡[a] Jing Li,‡[b] Yan Li,[a] Hong-Ping Long,[c] Wei Lin,[d] Yi-Kun Wang,[a] Rong Tang,[e] Xue-Wu Liu,[f] Dejian Jiang,[f] Shao Liu,[b] Dongsheng Cao,[a] Gui-Shan Tan,[b] Kang-Ping Xu[a] and Wen-Xuan Wang *[af]

Received 25th June 2024
Accepted 28th July 2024

DOI: 10.1039/d4ra04626a

rsc.li/rsc-advances

Hyperuricemia, characterized by elevated uric acid levels and subsequent crystal deposition, contributing to conditions such as gout, cardiovascular events, and kidney injury, poses a significant health threat, particularly in developed countries. Current drug options for treatment are limited, with safety concerns, leading to suboptimal therapeutic outcomes in symptomatic hyperuricemia patients and a lack of pharmaceutical interventions for asymptomatic cases. Distinguishing from the previous drug design strategies, we directly target uric acid, the pathological molecule of hyperuricemia, resulting in a pyrimidine derivative capable of increasing the solubility and excretion of uric acid by forming a complex with it. Its prodrug showed an anti-hyperuricemia activity comparable to benzbromarone and a favorable safety profile *in vivo*. Our finding provides a strategy purely based on organic chemistry to address the largely unmet therapeutic needs on novel anti-hyperuricemia drugs.

1. Introduction

Hyperuricemia, characterized by elevated uric acid (UA) concentrations in blood exceeding its solubility in water (approximately 420 μM), poses significant health risks, including the precipitation of urates in joints, kidneys, or urethra, leading to conditions such as gout, kidney injury, or urolithiasis.[1–3] Additionally, hyperuricemia is associated with an increased risk of various diseases, including stroke, hypertension, atherosclerosis, cardiovascular disease (CVD), and type 2 diabetes mellitus.[4–6] The prevalence of hyperuricemia is a growing concern globally, particularly in developed countries. For example, approximately 21% of the general population in the U.S. have asymptomatic hyperuricemia, and 3–4% experience gout.[7,8]

However, available agents for urate-lowering therapy, such as xanthine oxidase (XO) inhibitors, uricosuric agents, and uricase, are limited and carry severe side effects, including hepatotoxicity, nephrotoxicity, hypersensitivity, CVD-related death, nephrolithiasis, acute renal failure, or infusion reactions.[9–11] This has led to a conditional recommendation against initiating urate-lowering therapy in patients with asymptomatic hyperuricemia, including those with comorbid chronic kidney disease, CVD, urolithiasis, or hypertension,[9–11] leaving a significant gap in addressing the serious consequences of hyperuricemia.

Current efforts in developing anti-hyperuricemia drugs primarily focus on reducing UA generation by inhibiting XO or increasing excretion by inhibiting urate anion transporters.[11] However, targeting these functional proteins poses significant challenges due to potential serious side effects.[11–13] Furthermore, promoting UA excretion may also result in elevated UA concentration in urine, potentially increasing the risk of nephrolithiasis or kidney injury.[14–17] While urate oxidase offers a promising solution to remove excessive UA, its status as an exogenous protein limits its clinical application due to adverse reactions and immunogenicity.[11]

The only five FDA-approved urate-lowering drugs, namely allopurinol, febuxostat, probenecid, rasburicase, and pegloticase, all exhibit significant limitations.[18] Therefore, there is an urgent need for the development of novel drugs with enhanced therapeutic efficacy and reduced adverse effects. Despite a considerable number of urate-lowering drugs being in clinical development, there has been no breakthrough in their mechanisms, emphasizing the crucial need to explore novel anti-hyperuricemia strategies.

[a]*Xiangya School of Pharmaceutical Sciences, Central South University, Changsha, Hunan 410008, PR China. E-mail: wenxuanwang@tom.com*
[b]*Department of Pharmacy, National Clinical Research Center for Geriatric Disorder, Xiangya Hospital, Central South University, Changsha, Hunan 410008, PR China*
[c]*The First Hospital of Hunan University of Chinese Medicine, Changsha, Hunan 410007, PR China*
[d]*Department of Pathology, Xiangya Hospital, Central South University, Changsha, Hunan 410008, PR China*
[e]*Department of Nephrology, Xiangya Hospital, Central South University, Changsha, Hunan 410008, PR China*
[f]*Hunan Prima Drug Research Center Co., Ltd, Hunan Research Center for Drug Safety Evaluation, Hunan Key Laboratory of Pharmacodynamics and Safety Evaluation of New Drugs, Changsha, Hunan 410331, PR China*

† Electronic supplementary information (ESI) available. See DOI: https://doi.org/10.1039/d4ra04626a

‡ These authors contributed equally to this work.

The low solubility of urates in water plays a pivotal role in the formation of pathogenic crystalline. Designing a compound forming a more soluble complex with UA could alleviate the disease progression of hyperuricemia. Additionally, most UA is reabsorbed in the proximal tubule as a urate anion by organic anion transporters.[12,13] Introducing a cation that can form a neutral complex with it may facilitate UA escape from transportation. Therefore, directly targeting UA for anti-hyperuricemia drug design may achieve similar goals as inhibiting protein targets, while hopefully avoiding interference with physiological processes. Despite the absence of precedent examples of ligand-binding small molecular drugs, knowledge from base pairing of purines and pyrimidines in physiological environments, as well as the co-crystallization of UA and other heterocyclic compounds,[19] inspired the development of a novel anti-hyperuricemia agent directly targeting UA.

In this study, we present a small pyrimidine derivative as a binding partner for UA, capable of enhancing the solubility of urates and reducing ionization *in vitro*. Moreover, its prodrug demonstrated significant anti-hyperuricemia effects and low toxicity *in vivo*, offering a promising strategy for the development of novel anti-hyperuricemia drugs.

2. Results and discussion

2.1 Design, synthesis, and verification of a UA binding compound

The free energy per hydrogen bond of Watson–Crick base pairing in aqueous solution is roughly −1 to −2 kcal mol^{-1}.[20,21] UA, as a purine derivative, can also theoretically match a pyrimidine (*e.g.* 2,6-diaminopyridine) to form three hydrogen bonds like base pairing (Fig. 1a). Expecting to increase their affinity and water solubility of their complex, we substituted the two amino groups of 2,6-diaminopyridine by 2-hydroxy-ethyl groups to yield the structure of compound **1a**. To search the binding pattern between compound **1a** and UA, we performed molecular dynamics simulations for them with explicitly added water molecules, at a temperature (390 K) conducive to their free association and dissociation in several nano seconds, allowing us to explore as many possible conformations as we can. As a result, the dominating conformers of UA/**1a**-complex form five hydrogen bonds through 9′/12′-OH, 7′/10′-NH, and 1′-N of compound **1a** with the 6-CO, 7-NH, and 8-CO of UA, or unexpectedly, with the 8-CO, 1-NH, and 2-CO of UA (Fig. 1b). We then synthesized compound **1a** through the condensation reaction between 2-aminoethanol and 2,6-dichloropyrimidine. It turns out to be a hydrophilic weak base with log D (pH = 7.00) value of −0.65 and pK_a value of 7.51 at 25 °C (Scheme 1).

Because the dissolution and precipitation of a compound are dynamic equilibrium processes between the solution state and the solid state, the binding of compound **1a** with uric acid in the solution will reduce the number of free uric acid molecules, thereby promoting the balance to move towards dissolution, and the total level of uric acid in the solution will increase. Therefore, we can infer whether they are bound by measuring the solubility of uric acid in water. Due to the significant impact of the ionic strength of the solution on the solubility of uric acid, we used a low-ionic-strength buffer system (20 mM Et_3N/AcOH, pH = 7) to measure it in aqueous solutions containing different concentrations of compound **1a**. The results indicated that compound **1a** can significantly increase the solubility of uric acid in a dose-dependent manner (Fig. 1c).

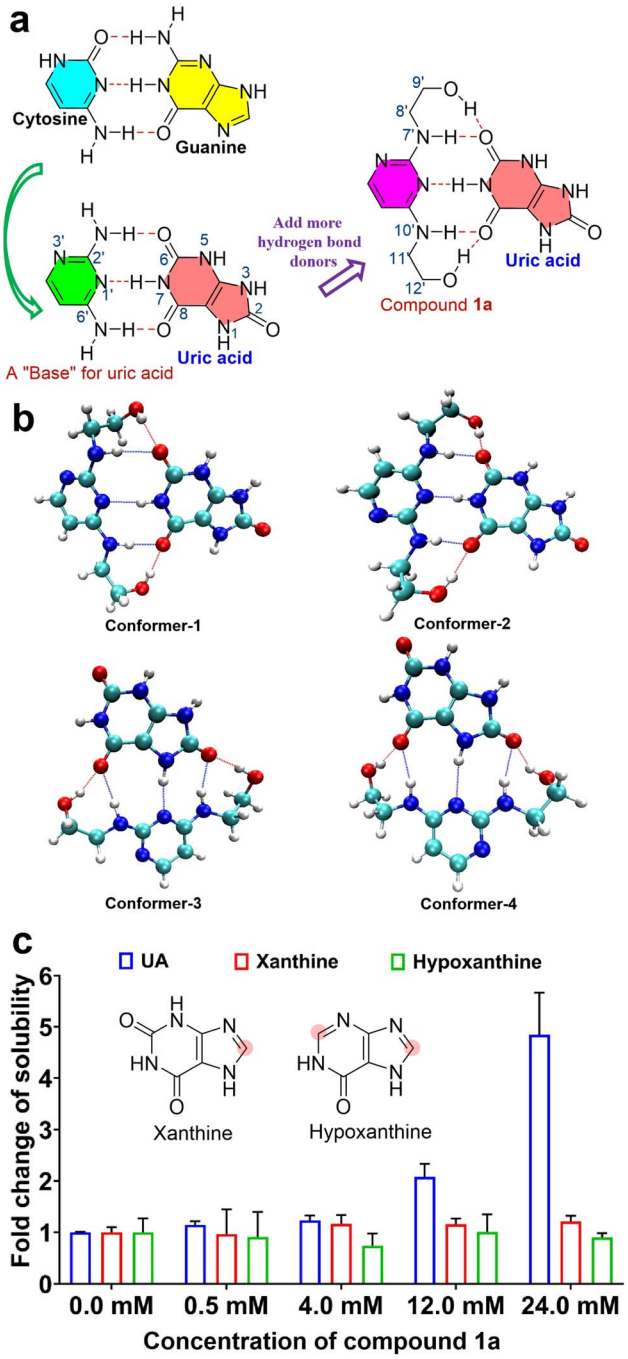

Fig. 1 Design of the compound (**1a**) with affinity to UA and the verification by molecular dynamic simulation and solubility-enhancement assay. (a) Designing compound **1a** from the idea of "base pairing". (b) The top 4 most frequently occurred configurations of compound **1a**/UA complex in 100 ns molecular dynamic simulation (balanced for 11 ns) at 390 K. (c) The fold change of solubility of UA, xanthine, and hypoxanthine in buffered solutions containing different concentration of compound **1a** (N = 3).

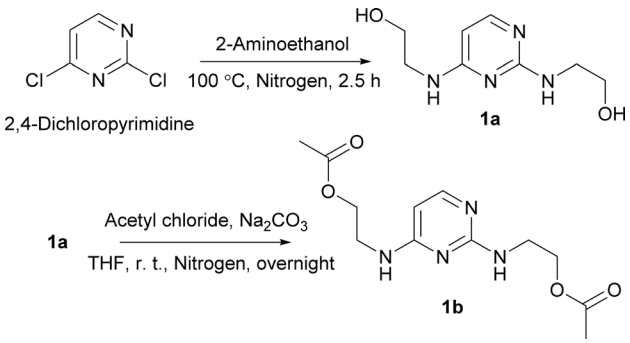

Scheme 1 Synthesis of compounds **1a** and **1b**.

To verify the binding conformation of compound **1a** and UA, we performed comparative experiments of two analogues of UA, namely xanthine and hypoxanthine. Xanthine, which is missing the 2-CO group, was expected to form conformers-1/-2 but not conformers-3/-4. While hypoxanthine, lacking both the 2-CO and 6-CO groups, should exhibit a diminished response to the concentration of compound **1a**. As a result, compound **1a** did not showed significant impact on the solubilities of xanthine and hypoxanthine at the concentration up to 40 mM, indicating that conformer-3/-4 should be their primary conformation in a neutral aqueous solution.

Additionally, we attempted to observe their binding status using NOESY spectroscopy. In the non-proton solvent DMSO-d_6, the signals of 1/3-NH of UA were disappeared, and those of 7/5-NH merged to one broad peak, when it was mixed with compound **1a** (1 : 1 ratio) (Fig. 2). A clear NOE correlation between the 9′/12′-OH of compound **1a** and the signal of UA was observable (Fig. 2c). We speculated that this is due to their spatial correlation between the 7-NH of uric acid and the 9′/12′-OH of compound **1a**, when they bind as conformer-3/4 (Fig. 2d). This result directly proves that they can form a complex. The conformer-1/-2 were ones of major conformers obtained from molecular dynamics simulation, but not supported by experimental results, possibly due to the lack of consideration for many complicated effects such as molecular ionization in the molecular dynamics simulation.

2.2 Affinity and the influence on solubility and ionization of UA

Subsequently, we determined the binding affinity between **1a** and UA in water at a pH value of 7.00 by conducting fluorescence enhancement assay, leading to the determination of K_d value of 61.4 ± 4.8 μM at 298.15 K, as well as a binding free energy of −5.75 ± 0.05 kcal mol^{-1} (Fig. 3a).[22] Without consideration on stacking conformations, the averaged free energy of

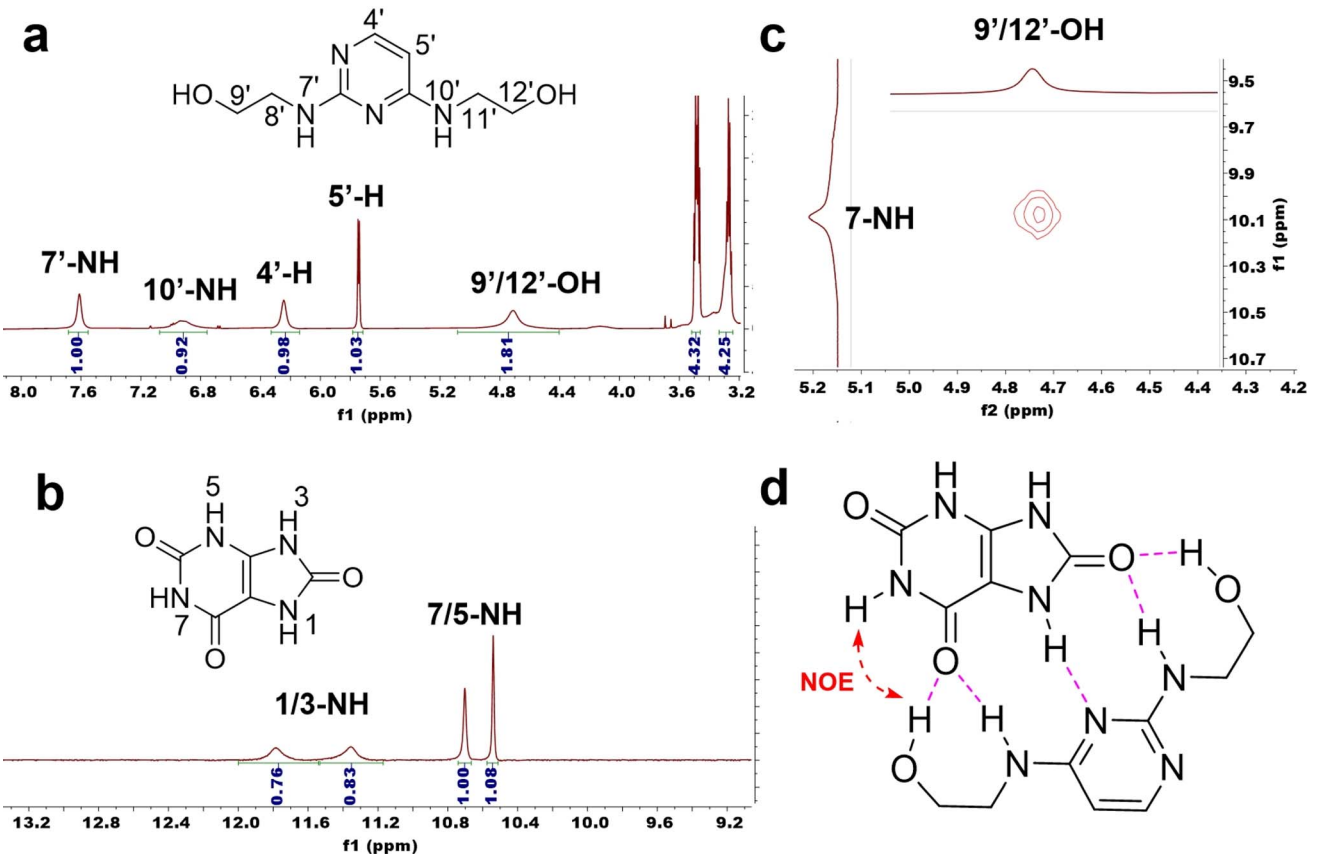

Fig. 2 NOESY experiment of the 1 : 1 mixture of compound **1a** and UA in DMSO-d_6. (a) the ^{1}H NMR spectrum of compound **1a** alone (600 MHz, DMSO-d_6). (b) the ^{1}H NMR spectrum of UA alone (600 MHz, DMSO-d_6). (c) The NOE cross peak between 9′/12′-OH of compound **1a** and 7-NH of UA. (d) Proposed conformation of complex, using conformer-3 for demonstration.

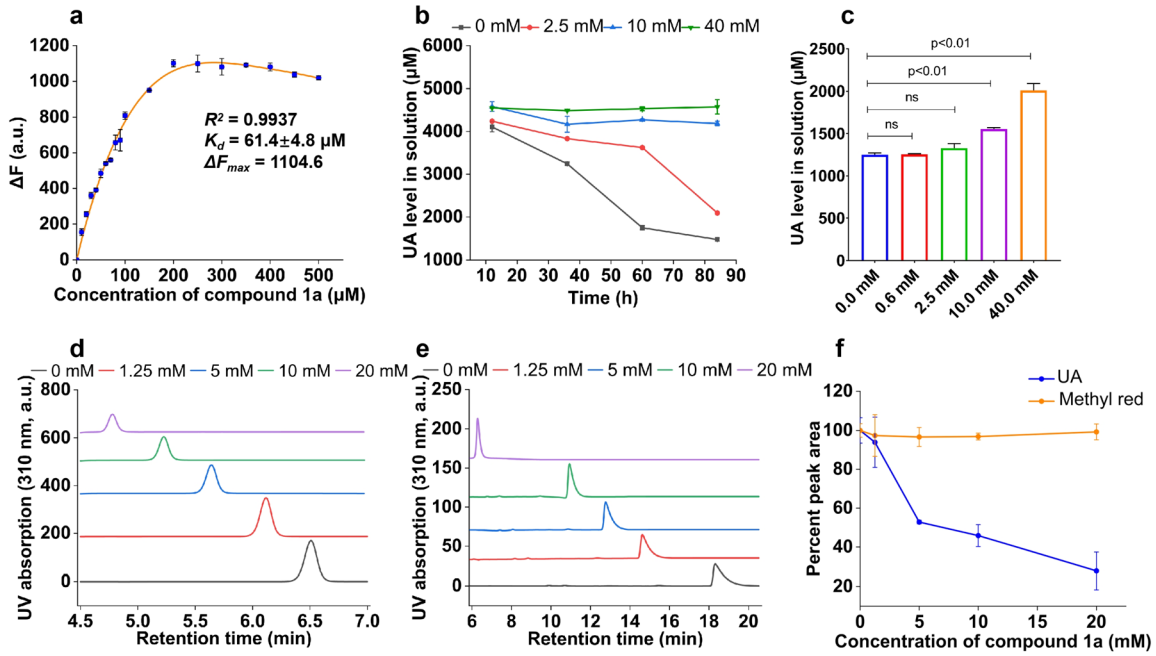

Fig. 3 The interactions between UA and compound **1a**. (a) Equilibrium binding of compound **1a** to UA measured by the increase in intrinsic fluorescence (ΔF) at 298.15 K ($N = 3$). Equilibrium dissociation constants (K_d) were then obtained by fitting data directly using nonlinear least squares analysis. (b) The change of the concentration of UA in UA-supersaturated solution (with 100 mM phosphate buffer, pH = 6.56) along with different total concentration of compound **1a** at 25 °C ($N = 3$). (c) Concentration of UA in buffer (5 mL 100 mM phosphate buffer, pH = 7.00, 25 °C) measured 12 h after the addition of excessive sodium urate crystals (4 mg) ($N = 3$). (d) The anion-exchange chromatography of UA using the mobile phases containing different concentrations of compound **1a**. (e) The anion-exchange chromatography of methyl red using the mobile phases containing different concentration of compound **1a**, as a negative control. (f) Peak area changes in the anion-exchange chromatography of UA and methyl red (negative control) when compound **1a** added in the mobile phase ($N = 3$).

forming one hydrogen bond is around −1.15 kcal mol^{-1}, similar to that of base pairs.

Poor solubility is an important pathogenic property of urates.[1,3,6] Binding to UA may interfere with their crystallization or precipitation from body fluids or glomerular filtrates. Consequently, we evaluated the impact of compound **1a** on the precipitation of supersaturated UA solution (25 °C) at the pH value of 6.56, which is the isoelectric point of compound **1a** and UA (pK_a 5.61)[23] and also close to the median pH value of urine[24] (Fig. 3b). When the total concentration of compound **1a** reached to 2.5 mM, the precipitation of UA was significantly inhibited. As the total concentration of compound **1a** increased to 40 mM and the UA molecules almost fully formed complex in solution, the solubility of total UA (4576.6 μM) was over 3 times that of UA alone (1472.5 μM) (Fig. 3b).

To simulate the effects on urates sediment in tissues, we assessed dissolution speed of sodium urate crystals in phosphate buffer with different concentration of compound **1a**. As a result, when the concentration of compound **1a** reaches to 10 mM, urate in solution is higher than blank buffer (Fig. 3c), implying that it could also accelerate the dissolution of tophus at a physiological condition.

At physiological pH, owing to the weak alkalinity of compound **1a**, its complexation with UA anions could form a neutrally charged complex, thereby potentially evading reabsorption mediated by organic anion transporters. With the aforementioned K_d value, for instance, over 90% UA molecules form complexes when the concentration of free compound **1a** exceeds 580 μM in neutral primary urine, implying that the reabsorption speed of UA could be reduced to 10–18% when the concentration of UA is below the K_m value of transporters according to the Michaelis–Menten equation. We have verified such effect of compound **1a** on UA by anion-exchange chromatography. The integrated area of UA anions on the anion exchange chromatography column gradually decreases as the increasing concentration of compound **1a** in the mobile phase, while the control ion, methyl red, shows no such effects (Fig. 3d–f). This experiment indicated that compound **1a** can selectively neutralize UA anion, and render it escape from the retention by the cations on the stationary phase.

Based on these experimental data, the concentration at which compound **1a** can exert its effects appears to be on the millimolar level. Despite it is a relatively high concentration, due to UA reabsorption and precipitation in urine is primarily within the kidney, the concentrating effect within the renal tubules may contribute to achieving an effective concentration of compound **1a** for anti-hyperuricemia activity with an acceptable administration dose.

2.3 Compound 1b showed anti-hyperuricemia activity *in vivo*

To assess the anti-hyperuricemia effects *in vivo*, we constructed the hyperuricemia mouse models following the well-established protocols.[25–27] Because compound **1a** is highly water-soluble,

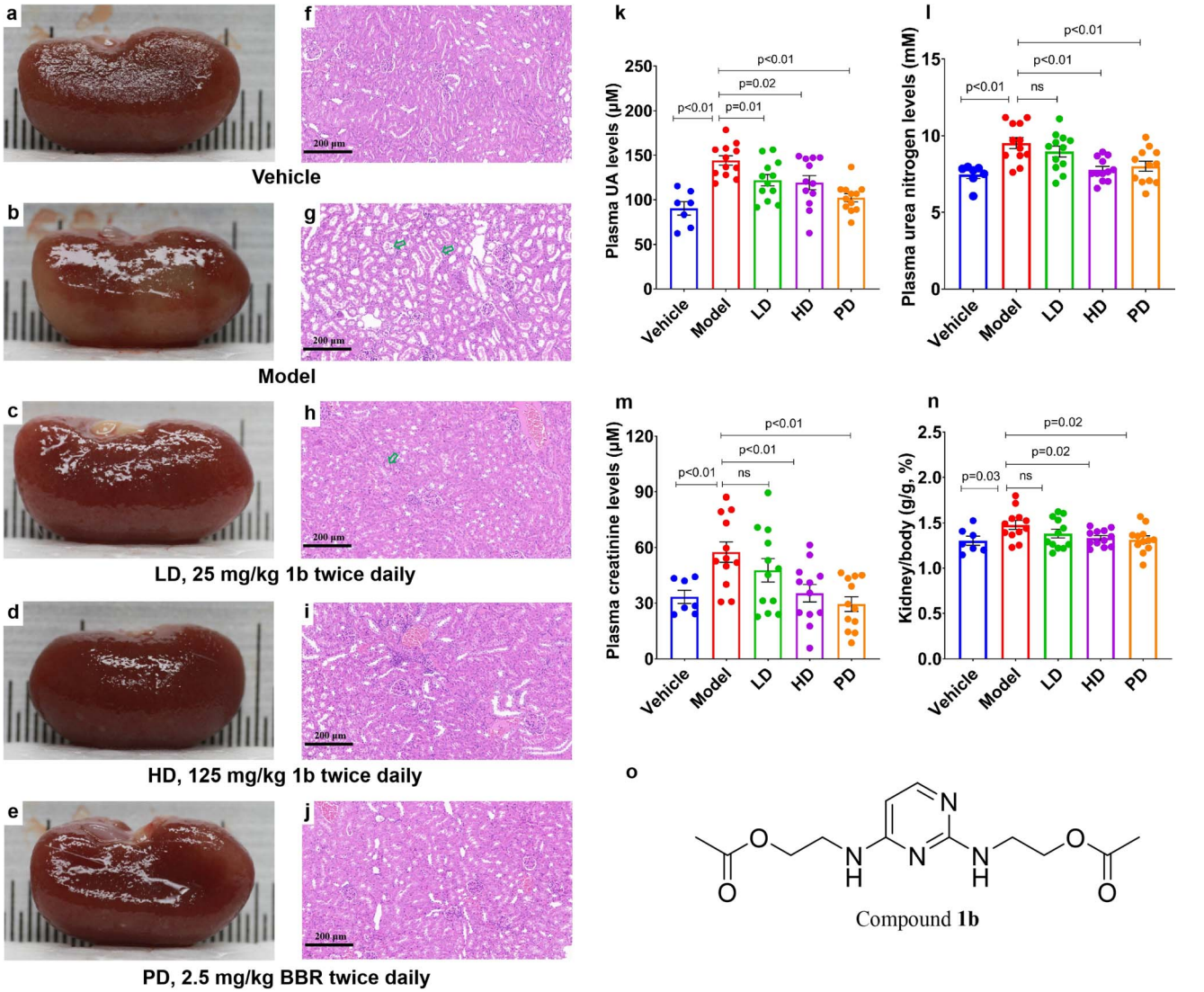

Fig. 4 The anti-hyperuricemia effects of compound **1b** and BBR on mouse model (vehicle, $n = 7$; others, $n = 12$). (a–e) The appearance of the representative kidneys. (f–j) Representative images of the kidney histology, H&E staining (×20, scale bar 200 μm). In the model group, tubular epithelial vacuolization with widespread loss of brush borders, accompanied by tubular dilation and the presence of granular casts within the tubular lumina can be observed as indicated by arrow. In LD group, focal loss of brush borders in renal tubules with individual tubular cells detaching can be observed as indicated by arrow. (k) Plasma UA levels. (l) Plasma urea nitrogen levels. (m) Plasma creatinine levels. (n) Kidney weight/body weight (g g^{-1}, %). (o) The structure of compound **1b**.

and may hardly be absorbed *via* oral administration, we used the fully acetylated product (**1b**, Fig. 4o) from **1a** as a prodrug in this assessment, which is a regular strategy applied for many prodrugs (*e.g.* famciclovir). We conducted a preliminary experiment on its excretion, and the results showed that 10.5 hours after oral administration of compound **1b**, over 40% was excreted through urine in the form of compound **1a**, thereby confirming that this prodrug strategy can ensure that **1a** reaches the kidneys and exerts its effect *in vivo* (Table S1†).

Due to the kidneys being one of the organs primarily affected by hyperuricemia, the renal function indicators of all groups were also evaluated, other than UA level in plasma (Fig. 4). With the administration of compound **1b**, the plasma UA levels of hyperuricemia mice in both high-dose (HD, 125 mg kg^{-1} twice daily) and low-dose (LD, 25 mg kg^{-1} twice daily) groups significantly reduced compared to the model group (Fig. 4k). Although the effect was not as strong as positive drug benzbromarone (BBR) (PD, 2.5 mg kg^{-1} twice daily), administration of high dose compound **1b** showed comparable protective effects on kidney, as read from the H&E staining kidney histology (Fig. 4a–j) and other renal function indicators (Fig. 4l–n).

2.4 Compound 1b showed low toxicity in acute toxicity test

We assessed the *in vivo* toxicity of compound **1b** in healthy Kunming mice with an oral dose of 2000 mg per kg per day for 14 days. In this administration period, no behavioral disorders, such as lethargy, clonic convulsion, anorexia, and ruffled fur, or other abnormal signs and symptoms were observed in both

vehicle and **1b**-treated groups. After dissection on all mouse corpses, there has no abnormalities in any organs observed by naked eyes. Moreover, we measured gains of body weight (Fig. 5a), weight of organs (Fig. 5b), the levels of alanine aminotransferase (ALT, Fig. 5c), and creatinine (Fig. 5d) in the plasma. No significant differences were observed between the vehicle group and **1b**-treated group, implying it has low influences on the physiological functions of mice. For comparison, the LD_{50} value of allopurinol, febuxostat, and benzbromarone are 700, 300, 618 mg kg^{-1} orally in mice, respectively.[28–30] The result showed that this new agent probably has a preferable safety profile.

3. Materials and methods

3.1 Materials

Proton nuclear magnetic resonance (^{1}H NMR) and carbon nuclear magnetic resonance (^{13}C NMR) spectra were recorded on a Bruker Avance 500 or Bruker Avance 600 NMR instrument in DMSO-d_6, methanol-d_4, or chloroform-d with tetramethylsilane (TMS) as an internal standard for all compounds. The coupling constant is expressed in hertz, and the chemical shift is expressed in the δ value (ppm) of TMS. The Agilent 6500 series Q-TOF was used for mass spectrometry measurements. The EnVision Microplate Reader was purchased from PerkinElmer Enterprises. The fluorescence spectrophotometer was Hitachi F-710 from Japan. The high-performance liquid chromatograph was purchased from Dalian Elite Analytical Instrument Co., Ltd. The Nano-300 micro-spectrophotometer was purchased from Hangzhou Aosheng Instrument Co., Ltd. The temperature of the reaction mixture was monitored with a thermostatic magnetic stirrer, purchased from Shanghai Sile Instrument Co., Ltd. The pH meter was lei magnetic PHS-3C, purchased from Shanghai INESA Scientific Instrument Co., Ltd. All reactions were routinely monitored using thin layer chromatography on silica gel GF254 plates purchased from Yantai Jiangyou Silica Gel Development Co., Ltd, and the spots were observed with potassium permanganate chromogenic solution or UV light irradiation (λ = 254 nm). The column layer chromatography method uses silica gel (200–300 mesh) packed column, which is purchased from Qingdao Yonghai Silica Gel Co., Ltd. Uric acid (UA, purity ≥98%) was purchased from Anhui Zesheng Technology Co., Ltd, and methyl red (purity ≥99%) was purchased from Shanghai Aladdin Biochemical Technology Co., Ltd. Potassium oxyazinate (purity ≥98%), hypoxanthine (purity ≥99%), and sodium carboxymethylcellulose (CMC-Na) were purchased from Shanghai Maclean's Biochemical Technology Co., Ltd. Benbromarone (BBR, purity ≥98%) was purchased from Shanghai Bichen Biochemical Technology Co., Ltd. Disodium ethylenediaminetetraacetate dihydrate (EDTA, purity ≥99%) was purchased from Sinopharm Chemical Reagent Co., Ltd. The assay kits for plasma UA (serial number: C012-2-1), plasma urea nitrogen (serial number: C013-2-1), plasma creatinine (serial number: C011-2-1), and plasma alanine aminotransferase (serial number: C009-2-1) were obtained from Nanjing Jiancheng Institute of Bioengineering. All other commercially available chemical reagents were chemically pure or analytically pure products and can be used directly without additional treatment unless otherwise specified. Phosphate buffer solution was prepared by adjusting 50 or 100 mM KH_2PO_4 solution to desired pH value with NaOH.

3.2 Animals

In this experiment, 8 week-old Kunming mice, weighing 40 ± 2 g, were purchased from Hunan Slack Jingda Laboratory Animal Co., Ltd (Hunan, China). All animal experimental procedures performed were in accordance with the "Animal Research: Reporting *in Vivo* Experiments" guidelines and approved by the Hunan Provincial Animal Experiment Management Committee (approval number: SYXK2019-0017, investigator number 20212281) and the Ethics Committee of Xiangya School of Pharmacy, Central South University. All mice were allowed free access to a standard diet and drinking water and were housed in an environment of 25 ± 2 °C, 60 ± 5% humidity, 12 h light/12 h dark cycle, and all mice were acclimatized to their living environment for one week prior to the experiments.

3.3 Synthesis of compound 1a and 1b

3.3.1 Compound 1a. 2,4-Dichloropyrimidine (100.00 mg, 0.67 mmol) was added to 2-aminoethanol (163.99 mg, 2.68 mmol) and reacted at 100 °C for 2.5 h under nitrogen protection. Then, the mixture was subjected to silica gel column chromatography with eluent CH_2Cl_2 : MeOH = 20 : 1 (v/v), and compound **1a** was obtained as a light yellow powder (yield: 63.91%). ^{1}H NMR (500 MHz, chloroform-d, 25 °C, TMS): δ 7.78 (d, 1H, J = 5.9 Hz, ArH), 5.77 (d, 1H, J = 5.9 Hz, ArH), 5.29 (br s, 1H, OH), 5.08 (br s, 1H, OH), 3.81–3.79 (m, 4H, CH_2), 3.54–3.50 (m, 4H, CH_2). ^{13}C NMR (150 MHz, DMSO-d_6, 25 °C, DMSO-d_6): δ 162.8, 162.2, 154.6, 95.9, 60.6, 59.9, 43.5, 42.6. ESI-HRMS (m/z): calcd for $C_8H_{15}N_4O_2$ $[M + H]^+$ 199.1190, found 199.1186.

3.3.2 Compound 1b. Compound **1a** (2.65 g, 13.31 mmol) was dissolved in anhydrous tetrahydrofuran (THF, 50 mL). Then dry Na_2CO_3 (4.23 g, 39.93 mmol) was added, and acetyl chloride (2.84 mL, 39.93 mmol) was slowly added dropwise. The reaction was carried out overnight at room temperature. Then the mixture was purified by silica gel column chromatography with eluent CH_2Cl_2 : MeOH = 15 : 1 (v/v) to yield compound **1b** as a yellow oil (yield: 77.45%). ^{1}H NMR (600 MHz, methanol-d_4, 25 °C, TMS): δ 7.58 (br s, 1H, ArH), 5.93 (d, J = 6.4 Hz, 1H, ArH), 4.22 (t, J = 5.7 Hz, 4H, CH_2), 3.67–3.62 (m, 4H, CH_2), 2.03 (m, 6H, CH_3). ^{13}C NMR (150 MHz, chloroform-d, 25 °C, TMS): δ 171.2, 170.6, 162.9, 162.0, 155.9, 95.4, 63.6, 63.2, 40.1, 39.7, 20.9, 20.8. ESI-HRMS (m/z): calcd for $C_{12}H_{19}N_4O_4$ $[M + H]^+$ 283.1401, found 283.1401.

3.4 Molecular dynamic simulation of UA and compound 1a in explicit solvation of water

The model was built by randomly adding one molecule of UA, one molecule of compound **1a**, and 56 molecules of water in a sphere with a radius of 8 Å. The system was optimized on GFN-FF level[31] by xTB 6.4.1,[32] then submitted for molecular dynamic simulation on GFN-FF level for 111 ns with parameters as following: temp. = 390 K, dump = 500 fs, step = 1.25 fs, hmass

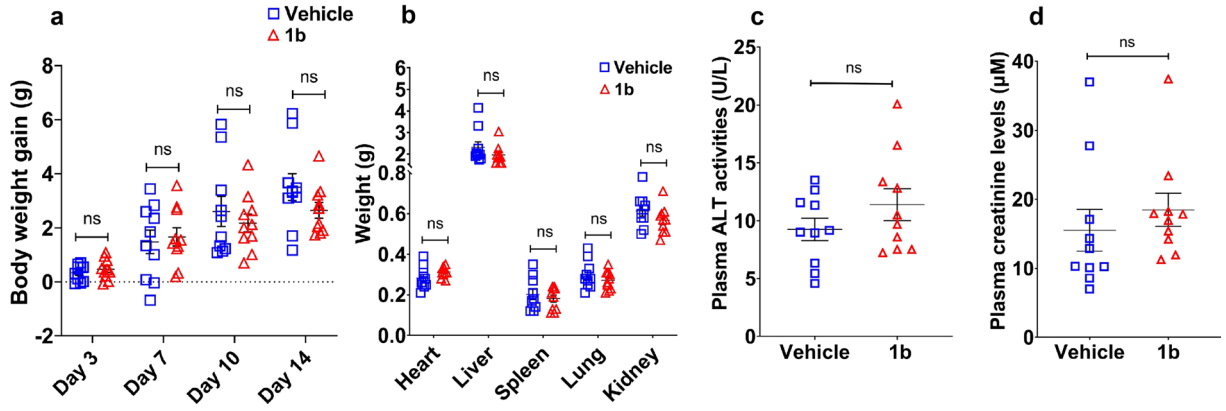

Fig. 5 The body weight gains, weights of organs, plasma ALT activity levels, and plasma creatinine levels of mice in vehicle group and compound **1b** (2000 mg kg^{-1} daily) administrated mice in 14 days acute toxicity assessment. (a) Body weight gains at day 3, day 7, day 10, and day 14. (b) The weights of their hearts, livers, spleens, lungs, and kidneys. (c) Plasma ALT activity levels. (d) Plasma creatinine levels.

= 4, shake = 2, *nvt* = true, potential = logfermi. We used the trajectory of the last 100 ns for analysis.

3.5 Solubility of UA, xanthine, and hypoxanthine in aqueous solution containing compound 1a

Because we found that at a higher temperature close to human body like 37 °C, uric acid in buffer solutions easily reached supersaturation and caused large deviations between parallel experiments, we conducted all the *in vitro* measurements at 25 °C, which is also common for the thermodynamic standard state.

At 25 °C, UA (33.6 mg), xanthine (7.6 mg), and hypoxanthine (6.8 mg) were added into 25 mL buffered solutions (20 mM Et_3N/AcOH, pH = 7.0) containing 0.0, 0.5, 4.0, 12.0, 24 mM compound **1a**, respectively. After stirring for 2 hours, the supernatant of each solution was taken after centrifugation, diluted by 20 times, and then analyzed with liquid chromatography. Based on the integrated area, the concentration of each analyte was calculated using its standard curves. The column was SinoChrom ODS-BP (3 μm, 2.1 mm × 100 mm). The retention time of UA was 5.4 min, with 100% water, 0.2 mL min^{-1}, detected by UV absorption at 293 nm. The retention time of xanthine was 4.3 min, with 100% water, 0.2 mL min^{-1}, detected by UV absorption at 267 nm. The retention time of hypoxanthine was 2.0 min, with 3% methanol, 0.2 mL min^{-1}, detected by UV absorption at 249 nm. The detected solubilities in blank buffered solution of UA, xanthine, and hypoxanthine were 1424.4, 243.5, 134.8 μM, respectively.

3.6 Fluorescence enhancement assay on affinity of UA and compound 1a

We assumed a stoichiometry of 1 : 1. The UA concentration was fixed at 40 μM, and the fluorescence enhancement of the complex was measured by varying the concentration of compound **1a**. Compound **1a** and UA were dissolved in a 100 mM phosphate buffer solution at pH value of 7.00 and 298.15 K. The concentration range of compound **1a** varied from 0 to 500 μM. The excitation wavelength for fluorescence was 293 nm, and the emission wavelength was 350 nm. The calculation of fluorescence enhancement was performed using the formula $I_{enhance} = I_{mix\_i} - I_{UA} - I_{\mathbf{1a}\_i}$, where $I_{enhance}$, I_{mix_i}, I_{UA} and $I_{\mathbf{1a}\_i}$ represent the fluorescence intensity enhancement with compound **1a** with at concentration *i*, the fluorescence intensity of the mixture of 40 μM UA and compound **1a** at concentration *i*, the fluorescence intensity of 40 μM UA alone, and the fluorescence intensity of compound **1a** at concentration *i* alone, respectively. After measurements, a plot was generated with the concentrations of compound **1a** on the *x*-axis and fluorescence enhancement on the *y*-axis. A curve was fitted using unbiased fourth-degree polynomial by nonlinear least squares method. The maximum fluorescence enhancement was determined to be 1104.5 a.u., and the concentration of compound **1a** corresponding to half-maximal fluorescence enhancement was 61.4 ± 4.8 μM, thus yielding a K_d value of 61.4 ± 4.8 μM. The standard errors of K_d and binding free energy were estimated by error propagation from the variances in measurements.

3.7 Inhibition on UA precipitation by compound 1a

Different concentrations of compound **1a** (0.0, 2.5, 10.0, 40.0 mM) were dissolved in 5 mL of 100 mM phosphate buffer solution (pH = 6.56), respectively. Excess UA was added to each solution, and they were saturated in a water bath at 80 °C, followed by filtration and subsequent cooling to 25 °C. Supernatants of each buffered solution were collected at 12, 36, 60, and 84 hours. These supernatants were then diluted and their absorbance was measured at 293 nm using a UV-vis spectrophotometer, with UA-free buffer solutions containing corresponding concentrations of compound **1a** serving as blanks. UA concentrations were determined using a standard curve relating UA concentration to UV absorbance in the buffer solution.

3.8 Dissolution of sodium urate by compound 1a

Compound **1a** was dissolved in 5 mL of 100 mM phosphate buffer solution (pH = 7.00) to yield solutions with different concentrations of **1a** (0.0, 0.6, 2.5, 10.0, 40.0 mM). 4 mg crystals of sodium urate monohydrate were added to each solution, and they were stirred at 25 °C. Supernatants of each buffered solution were collected after 12 hours, and then were diluted and measured for absorbance at 293 nm using a UV-vis

spectrophotometer, with UA-free buffer solutions containing corresponding concentrations of compound **1a**. UA concentrations were determined using a standard curve relating UA concentration to UV absorbance in the buffer solution.

3.9 Anion exchange chromatography of UA and methyl red with compound 1a in mobile phase

The experiments were conducted using Ultimate XB-SAX HPLC column (5 μm, 4.6 × 250 mm) and mobile phase of 20 mM triethylamine/acetic acid buffer solution (pH = 6.50, 1 mL min^{-1}, 0–25 min) containing compound **1a** with concentrations of 0.00, 1.25, 5.00, 10.00, 20.00 mM, respectively. The chromatography was recorded by UV absorption at 310 nm. The inject volume of standard samples of UA (400 μM) and methyl red (100 μM) was 40 μL.

3.10 Measurement of log *D*

Compound **1a** (100 mg) was dissolved in 25 mL 50 mM phosphate buffer (at 25 °C, pH = 7.00), and 25 mL *n*-octanol then added. The system was stirred and balanced. The concentrations of **1a** in water and *n*-octanol were determined by UV absorption at 219 nm using the standard curves relating concentration to UV absorbance in the corresponding solution. log *D* value was calculated by formula $\log D = \log(C_{n\text{-o}}/C_{\text{w}})$, where $C_{n\text{-o}}$ and C_{w} were the concentration of **1a** in *n*-octanol and water, respectively.

3.11 Measurement of pK_a

At 25 °C, the 25 mL 0.01 M solution of compound **1a** was adjusted into pH = 9.34 with 0.1 M NaOH solution. Then 100 μL 0.1 M HCl solution was stepwise added to the system, and the pH value was monitored by a pH meter, till the pH value was 5.64. Titration curves were constructed by plotting the volume of added hydrochloric acid solution on the *y*-axis against the corresponding pH values on the *x*-axis. The inflection point of the curve, where the absolute value of the first derivative was maximal, was found to be at pH 7.51. Consequently, the pK_a of the compound was determined to be 7.51 (Fig. S6†).

3.12 *In vivo* anti-hyperuricemia assay

This experiment was performed in a blinded fashion. All the agents used in this experiment were dissolved or suspended in 0.9% saline containing 0.5% CMC-Na. After one week of acclimatization, 55 8 week-old male Kunming mice were randomly divided into 5 groups: HD group (125 mg per kg **1b** twice daily, $n = 12$), LD group (25 mg per kg **1b** twice daily, $n = 12$), PD group (2.5 mg per kg BBR twice daily, $n = 12$), model group ($n = 12$), and vehicle group ($n = 7$). The daily dosing regimen was conducted sequentially over time. In the first hour, the mice in HD, LD, and PD groups were orally gavaged with 125 mg per kg **1b** (0.1 mL), 25 mg per kg **1b** (0.1 mL), and 2.5 mg per kg BBR (0.1 mL), respectively. Meanwhile, the mice in model and vehicle group were given the same volume of blank carrier solution. In the second hour, the mice in HD, LD, PD, and model groups were orally gavaged with 300 mg per kg hypoxanthine (0.2 mL), while the mice in vehicle group was given a blank carrier solution (0.2 mL). In the third hour, the mice in HD, LD, PD, and model groups were intraperitoneally injected with 300 mg per kg potassium oxyzinate (0.2 mL), while the mice in vehicle group were given the same volume of blank carrier solution. In the fourth hour, the mice in HD, LD, and PD groups were orally gavaged with 125 mg per kg **1b** (0.1 mL), 25 mg per kg **1b** (0.1 mL), and 2.5 mg per kg BBR (0.1 mL) for the second time, respectively, while the mice in model and vehicle group were given the same volume of blank carrier solution. The administration cycles last for 8 days. One hour after the final administration on the 8th day, mice in each group were weighed. Then, blood sample was collected from the orbital sinus and stored in tubes with 1 mg per mL EDTA, and centrifugated at 3000 rpm for 10 minutes at 4 °C to yield the plasma. Subsequently, the mice were immediately euthanized by cervical dislocation, and the kidneys were weighed and photographed, and then fixed separately in 4% paraformaldehyde solution. UA, urea nitrogen, and creatinine levels in plasma were measured using assay kits according to the manufacturer's instructions.

Tissues of the right kidney were treated with paraformaldehyde (4%) for 24 h, then dehydrated, immersed in wax and embedded, and then sectioned (4 μm) for H&E staining. Through the scanning and browsing software (3DHISTECH (Hungary) CaseViewer 2.4), the tissue sections were observed in detail at different folds.

3.13 *In vivo* acute toxicity test

This experiment was not performed in a blinded fashion. The design of experiment refers to "The Guiding Principles for Acute Toxicity Testing of Chemical Drugs, GPT1-1" that approved by National Medical Products Administration of China. After one week of acclimatization, mice are randomly divided into 2 groups: a dosing group ($n = 10$, 5 females, 5 males), and a vehicle group ($n = 10$, 5 females, 5 males). For daily administration, mice in dosing group were orally gavaged by 2000 mg kg^{-1} (suspended in 0.3 mL 0.9% saline) compound **1b**, and the mice in vehicle group were given the same volume of 0.9% saline. The administration cycles last for 14 days. The body weight of mice was recorded at the 1st, 3rd, 7th, 10th, and 14th days. One hour after the administration on the 14th dosing day, all the mice were weighed, and the blood was collected from the orbital sinus, and then they were immediately euthanized by cervical dislocation. Blood samples were stored in tubes with 1 mg per mL EDTA, and centrifugated at 3000 rpm for 10 minutes at 4 °C to yield plasma. The organs, including hearts, livers, spleens, lungs and kidneys, were obtained by dissecting mice, and then they were photographed, examined, and fixed with 4% paraformaldehyde. ALT activity levels and creatinine in plasma were measured using assay kits according to the manufacturer's instructions.

3.14 Statistical analysis

Data were expressed as mean ± standard error (mean ± SEM). One-way ANOVA was used to determine the significant differences between groups, and $p > 0.05$ was determined to be "not

significant" (ns). In the figure legends, n = the number of independent biological replicates (animals), and N = the number of independent experimental replicates.

4. Conclusion

Herein, our work introduces a novel strategy of designing a "binding partner" for the treatment of hyperuricemia, purely based on the basic rules of organic chemistry. We bound UA by an easily obtainable, non-immunogenic small molecule to achieve the goals of enhancing the solubility and excretion of UA. Although compound **1a** exhibits weaker affinity to UA compared to that level of drug–protein interactions, and shows efficacy at concentrations of several millimoles, it still has anti-hyperuricemia effects *in vivo* probably due to the concentrating effect in the renal tubules. With high water solubility and no specific design for functional proteins, it exhibits the potential to minimize side effects, as we observed in acute toxicity testing. Moreover, its characteristics in increasing urates' solubility suggest possible co-administration with other uricosuric drugs, to reduce the risk of UA precipitation in the kidneys and offer potential application in patients with kidney stones.

Compound **1a** is a preliminary design that forms only at most 5 hydrogen bonds with UA. Since UA has three hydrogen bond acceptors and four donors, future improvements aiming to enhance the affinity to UA could be achieved by increasing the number of intermolecular hydrogen bonds. For instance, if a compound can form 7 intermolecular hydrogen bonds with UA, the K_d (298.15 K) value of the complex will fall down to nanomolar level, as one hydrogen bond contributes -1.15 kcal mol^{-1} free energy in aqueous solution in our findings. Such bind partner of UA will act throughout the body fluids, thereby additionally raising the alert threshold for blood UA level, with the hope of transforming hyperuricemia into a chronically manageable condition.

We believe that the strategy of binding ligand molecules can also provide new clues for the development of other small molecule drugs, distinct from traditional drug development strategies that target large biomolecules.

Data availability

All data generated or analyzed during this study are included in this article and its ESI† files. The datasets used and/or analyzed during the current study are available from the corresponding author on reasonable request.

Author contributions

Conceptualization: W.-X. W. Methodology: Y.-Y. L., J. L., Y. L., H.-P. L., W. L., Y.-K. W., R. T., X.-W. L., D. J., S. L., D. C., G.-S. T., K.-P. X. Investigation: Y.-Y. L., J. L. Visualization: W.-X. W., Y.-Y. L. Funding acquisition: W.-X. W., J. L., Y.-Y. L. Project administration: W.-X. W. Supervision: W.-X. W., J. L. Writing original draft: W.-X. W., Y.-Y. L. Review and editing: J. L. Y.-Y. L. and J. L. contributed equally.

Conflicts of interest

The authors declare no competing financial interest.

Acknowledgements

The authors thank the Institute for Advanced Study, Central South University for NMR measurement. This work was supported by National Natural Science Foundation of China (82173713), Key Research and Development Program of Hunan Province (2022SK2031), Natural Science Foundation of Hunan Province (2024JJ8127), and Graduate Innovation Project of Hunan Province (CX20230323).

References

1 R. J. Johnson, G. L. Bakris, C. Borghi, M. B. Chonchol, D. Feldman, M. A. Lanaspa, T. R. Merriman, O. W. Moe, D. B. Mount, L. G. S. Lozada, E. Stahl, D. E. Weiner and G. M. Chertow, Hyperuricemia, acute and chronic kidney disease, hypertension, and cardiovascular disease: report of a scientific workshop organized by the national kidney foundation, *Am. J. Kidney Dis.*, 2018, **71**(6), 851–865.

2 R. J. Johnson, T. Nakagawa, D. Jalal, L. G. Sánchez-Lozada, D.-H. Kang and E. Ritz, Uric acid and chronic kidney disease: which is chasing which?, *Nephrol., Dial., Transplant.*, 2013, **28**(9), 2221–2228.

3 J. Miake, I. Hisatome, K. Tomita, T. Isoyama, S. Sugihara, M. Kuwabara, K. Ogino and H. Ninomiya, Impact of hyper- and hypo-uricemia on kidney function, *Biomedicines*, 2023, **11**(5), 1258.

4 D. I. Feig, D.-H. Kang and R. J. Johnson, Uric acid and cardiovascular risk, *N. Engl. J. Med.*, 2008, **359**(17), 1811–1821.

5 A. Maloberti, A. Mengozzi, E. Russo, A. F. G. Cicero, F. Angeli, E. A. Rosei, C. M. Barbagallo, B. Bernardino, M. Bombelli, F. Cappelli, E. Casiglia, R. Cianci, M. Ciccarelli, M. Cirillo, P. Cirillo, G. Desideri, L. D'Elia, R. Dell'Oro, R. Facchetti, C. Ferri, F. Galletti, C. Giannattasio, L. Gesualdo, G. Iaccarino, L. Lippa, F. Mallamaci, S. Masi, M. Masulli, A. Mazza, M. L. Muiesan, P. Nazzaro, G. Parati, P. Palatini, P. Pauletto, R. Pontremoli, N. R. Pugliese, F. Quarti-Trevano, M. Rattazzi, G. Reboldi, G. Rivasi, M. Salvetti, V. Tikhonoff, G. Tocci, A. Ungar, P. Verdecchia, F. Viazzi, M. Volpe, A. Virdis, G. Grassi and C. Borghi, Working Group on Uric Acid and Cardiovascular Risk of the Italian Society of Hypertension, The results of the URRAH (uric acid right for heart health) project: a focus on hyperuricemia in relation to cardiovascular and kidney disease and its role in metabolic dysregulation, *High Blood Pressure Cardiovasc. Prev.*, 2023, **30**(5), 411–425.

6 M. I. Ahmad, S. Masood, D. M. Furlanetto and S. Nicolaou, Urate crystals; beyond joints, *Front. Med.*, 2021, **8**, 649505.

7 L. Li, Y. Zhang and C. Zeng, Update on the epidemiology, genetics, and therapeutic options of hyperuricemia, *Am. J. Transl. Res.*, 2020, **12**(7), 3167–3181.

8 M. Dehlin, L. Jacobsson and E. Roddy, Global epidemiology of gout: prevalence, incidence, treatment patterns and risk factors, *Nat. Rev. Rheumatol.*, 2020, **16**(7), 380–390.

9 J. D. FitzGerald, N. Dalbeth, T. Mikuls, R. Brignardello-Petersen, G. Guyatt, A. M. Abeles, A. C. Gelber, L. R. Harrold, D. Khanna, C. King, G. Levy, C. Libbey, D. Mount, M. H. Pillinger, A. Rosenthal, J. A. Singh, J. E. Sims, B. J. Smith, N. S. Wenger, S. S. Bae, A. Danve, P. P. Khanna, S. C. Kim, A. Lenert, S. Poon, A. Qasim, S. T. Sehra, T. S. K. Sharma, M. Toprover, M. Turgunbaev, L. Zeng, M. A. Zhang, A. S. Turner and T. Neogi, 2020 American College of Rheumatology Guideline for the Management of Gout, *Arthritis Rheumatol.*, 2020, **72**(6), 879–895.

10 T. Neogi, Gout, *N. Engl. J. Med.*, 2011, **364**(5), 443–452.

11 X. Zeng, Y. Liu, Y. Fan, D. Wu, Y. Meng and M. Qin, Agents for the treatment of gout: current advances and future perspectives, *J. Med. Chem.*, 2023, **66**(21), 14474–14493.

12 S. K. Nigam, K. T. Bush, G. Martovetsky, S.-Y. Ahn, H. C. Liu, E. Richard, V. Bhatnagar and W. Wu, The organic anion transporter (OAT) family: a systems biology perspective, *Physiol. Rev.*, 2015, **95**(1), 83–123.

13 E. M. Quistgaard, C. Löw, F. Guettou and P. Nordlund, Understanding transport by the major facilitator superfamily (MFS): structures pave the way, *Nat. Rev. Mol. Cell Biol.*, 2016, **17**(2), 123–132.

14 T. Taniguchi, N. Ashizawa, K. Matsumoto, R. Saito, K. Motoki, M. Sakai, N. Chikamatsu, C. Hagihara, M. Hashiba and T. Iwanaga, Pharmacological evaluation of dotinurad, a selective urate reabsorption inhibitor, *J. Pharmacol. Exp. Ther.*, 2019, **371**(1), 162–170.

15 A. Novikov, Y. Fu, W. Huang, B. Freeman, R. Patel, C. van Ginkel, H. Koepsell, M. Busslinger, A. Onishi, J. Nespoux and V. Vallon, SGLT2 inhibition and renal urate excretion: role of luminal glucose, GLUT9, and URAT1, *Am. J. Physiol.: Renal Physiol.*, 2019, **316**(1), F173–F185.

16 S. O. Ahn, S. Ohtomo, J. Kiyokawa, T. Nakagawa, M. Yamane, K. J. Lee, K. H. Kim, B. H. Kim, J. Tanaka, Y. Kawabe and N. Horiba, Stronger uricosuric effects of the novel selective URAT1 inhibitor UR-1102 lowered plasma urate in tufted capuchin monkeys to a greater extent than benzbromarone, *J. Pharmacol. Exp. Ther.*, 2016, **357**(1), 157–166.

17 M. Hosoyamada, Y. Tsurumi, H. Hirano, N. H. Tomioka, Y. Sekine, T. Morisaki and S. Uchida, Urat1-Uox double knockout mice are experimental animal models of renal hypouricemia and exercise-induced acute kidney injury, *Nucleosides, Nucleotides Nucleic Acids*, 2016, **35**(10–12), 543–549.

18 C. Jenkins, J. H. Hwang, J. B. Kopp, C. A. Winkler and S. K. Cho, Review of Urate-Lowering Therapeutics: From the Past to the Future, *Front. Pharmacol*, 2022, **13**, 925219.

19 V. M. Hall, A. Thornton, E. K. Miehls, J. A. Bertke and J. A. Swift, Uric Acid Crystallization Interrupted with Competing Binding Agents, *Cryst. Growth Des.*, 2019, **19**, 7363–7371.

20 E. Stofer, C. Chipot and R. Lavery, Free Energy Calculations of Watson−Crick Base Pairing in Aqueous Solution, *J. Am. Chem. Soc.*, 1999, **121**, 9503–9508.

21 S. M. Freier, N. Sugimoto, A. Sinclair, D. Alkema, T. Neilson, R. Kierzek, M. H. Caruthers and D. H. Turner, Stability of XGCGCp, GCGCYp, and XGCGCYp helixes: an empirical estimate of the energetics of hydrogen bonds in nucleic acids, *Biochemistry*, 1986, **25**(11), 3214–3219.

22 T. D. Pollard, A guide to simple and informative binding assays, *Mol. Biol. Cell*, 2010, **21**(23), 4061–4067.

23 B. Finlayson and A. Smith, Stability of first dissociable proton of uric acid, *J. Chem. Eng. Data*, 1974, **19**, 94–97.

24 V. Walker, Chapter Four - Phosphaturia in kidney stone formers: Still an enigma, *Adv. Clin. Chem.*, 2019, **90**, 133–196.

25 L.-C. Cheng, V. Murugaiyah and K.-L. Chan, Flavonoids and phenylethanoid glycosides from Lippia nodiflora as promising antihyperuricemic agents and elucidation of their mechanism of action, *J. Ethnopharmacol.*, 2015, **176**, 485–493.

26 T. Yong, M. Zhang, D. Chen, O. Shuai, S. Chen, J. Su, C. Jiao, D. Feng and Y. Xie, Actions of water extract from Cordyceps militaris in hyperuricemic mice induced by potassium oxonate combined with hypoxanthine, *J. Ethnopharmacol.*, 2016, **194**, 403–411.

27 M. Lu, J. Yin, T. Xu, X. Dai, T. Liu, Y. Zhang, S. Wang, Y. Liu, H. Shi, Y. Zhang, F. Mo, V. Sukhorukov, A. N. Orekhov, S. Gao, L. Wang and D. Zhang, Fuling-Zexie formula attenuates hyperuricemia-induced nephropathy and inhibits JAK2/STAT3 signaling and NLRP3 inflammasome activation in mice, *J. Ethnopharmacol.*, 2024, **319**(Pt2), 117262.

28 *Product Information, ZYLOPRIM® (allopurinol)*, **https://www.accessdata.fda.gov/drugsatfda_docs/label/2018/016084s044lbl.pdf**.

29 *Drugbank: Febuxostat*, **https://go.drugbank.com/drugs/DB04854**.

30 *Pubchem: Benzbromarone*, **https://pubchem.ncbi.nlm.nih.gov/compound/2333**.

31 S. Spicher and S. Grimme, Robust Atomistic Modeling of Materials, Organometallic, and Biochemical Systems, *Angew Chem. Int. Ed. Engl.*, 2020, **59**(36), 15665–15673.

32 C. Bannwarth, E. Caldeweyher, S. Ehlert, A. Hansen, P. Pracht, J. Seibert, S. Spicher and S. Grimme, Extended tight-binding quantum chemistry methods, *Wiley Interdiscip. Rev.: Comput. Mol. Sci.*, 2021, **11**, e1493.